Supporting Information

Molecular imaging of Sirtuin1 expression-activity in the rat brain using positron emission tomography/magnetic resonance imaging (PET/MRI) with [^{18}F]-2-fluorobenzoylaminohexanoicanilide.

Robin Bonomi[a,b], Vadim Popov[a,b], Maxwell Laws[a,b], David Gelovani[a,b], Anjoy Majhi[a,b], Aleksandr Shavrin[a,b], Xin Lu[b,c], Otto Muzik[b,c], Nashaat Turkman[a,b], Renshyan Liu[d], Thomas Mangner[b,c], Juri G. Gelovani[a,b]*

Table of Contents

Table S1. Table of end point assay *Kcat* values for focused library of compounds with SIRT1-7 (60 minute time point). Values represented as $* \, 10^{-3} \; per \; second$.

Number	Leaving Group	Sirt1	Sirt2	Sirt3	Sirt4	Sirt5	Sirt6	Sirt7
1	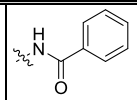	0.41 ± 0.014	0.018 ± 0.002	0.298 ± 0.002	0.07 ± 0.003	0.08 ± 0.001	0.14 ± 0.003	NR
2	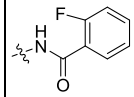	1.13 ± 0.064	0.009 ± 0.001	0.29 ± 0.106	0.13 ± 0.02	0.24 ± 0.027	NR	NR
3	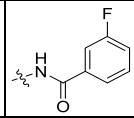	0.33 ± 0.030	0.01 ± 0.0001	0.063 ± 0.012	0.03 ± 0.005	0.07 ± 0.003	0.16 ± 0.028	0.013 ± 0.016
4	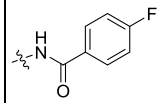	1.41 ± 0.509	0.01 ± 0.118	0.05 ± 0.136	0.15 ± 0.070	0.02 ± 0.001	0.24 ± 0.058	NR
5	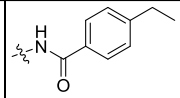	0.64 ± 0.041	0.015 ± 0.004	0.116 ± 0.072	0.04 ± 0.004	0.85 ± 0.009	0.18 ± 0.017	0.017 ± 0.001
6	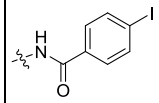	0.01 ± 0.001	0.004 ± 0.001	0.007 ± 0.004	0.02 ± 0.002	NR	NR	NR
7	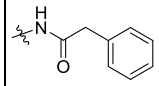	0.37 ± 0.020	0.006 ± 0.020	0.13 ± 0.029	0.06 ± 0.004	NR	NR	NR
8	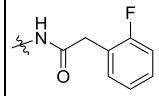	0.05 ± 0.012	NR	0.02 ± 0.033	NR	NR	NR	NR
9	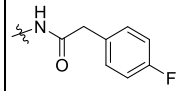	0.11 ± 0.071	0.02 ± 0.001	0.09 ± 0.008	0.06 ± 0.036	0.06 ± 0.002	0.13 ± 0.021	0.04 ± 0.017
10	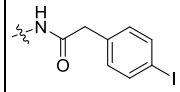	0.12 ± 0.027	0.04 ± 0.025	0.01 ± 0.003	0.01 ± 0.006	NR	NR	NR

Table S2. Michaelis-Menten kinetic parameters for SIRT1 with specific compounds. Intermediate reaction time points were measured at 5, 15, 30, 60 minutes post reaction initiation. The leaving groups are labeled in the top line of the table.

Parameter/Compound	1	2	3	4	7	8	BPS1
Vmax (uM/sec)	0.015	0.102	0.373	0.028	0.051	0.294	0.536
Stand. Dev.	4.32E-04	3.53E-02	1.81E-02	3.33E-03	5.27E-03	6.36E-03	2.83E-01
km(uM)	91.99	239.16	358.95	104.84	147.96	940.38	500.34
Stand. Dev.	2.70	82.71	17.41	12.61	15.32	20.34	264.45
kcat (per sec)	0.0009	0.0062	0.0228	0.0017	0.0031	0.0179	0.0327
Stand. Dev.	2.56E-05	2.09E-03	1.07E-03	1.97E-04	3.12E-04	3.76E-04	1.68E-02
kcat/km (per sec, M)	9.75	26.02	63.39	16.08	21.00	19.06	65.29
Stand. Dev.	0.37	7.07	4.32	1.32	1.22	0.58	6.21

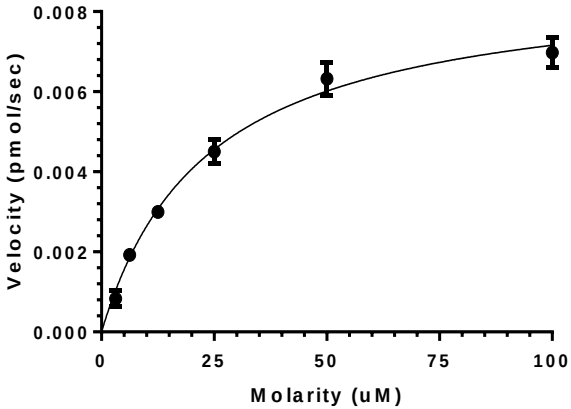

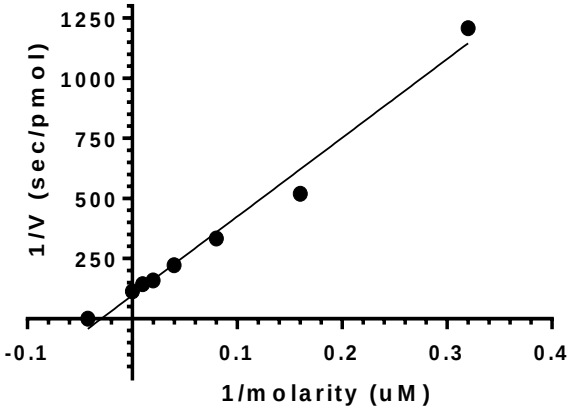

Table S3. Table of PET SUV values for 2[^{18}F]BzAHA in specific ROI's of the brain.

	Rostral Hippocampus	Caudal Hippocampus	Amygdala	LSN	N. Accumbens	Cerebellum	Cortex	Brainstem	Muscle
SUV at 15 min	0.683±0.0745	0.644±0.045	0.668±0.023	0.6±0.0863	0.618±0.044	0.33±0.021	0.453±0.161	0.236±0.038	0.219±0.075
SUV norm by brainstem	2.97±0.803	2.80±0.642	2.87±0.363	2.62±0.728	2.64±0.258	1.42±0.288	2.02±1.03	1	0.962±0.454
Influx Rate Constant *(Ki)*	0.0449±0.0071	0.0507±0.0075		0.0487±0.0025	0.0327±0.0061	0.00297±0.0039			

Figure S1A. ^{19}F NMR spectra for 2-FBzAHA

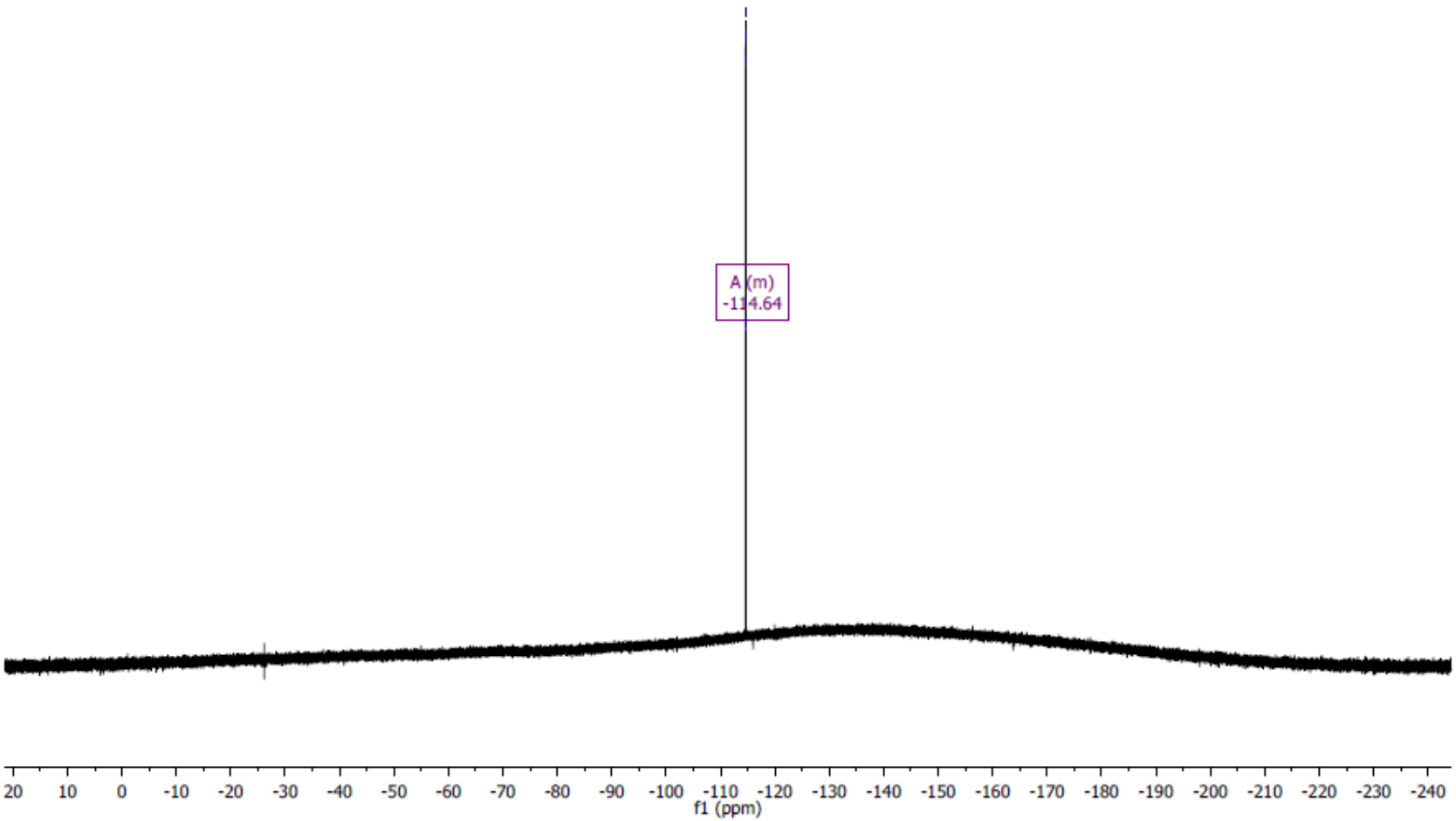

Figure S1B. ^{19}F NMR spectra for 2F-benzoic acid, with peak at -113.00 ppm.

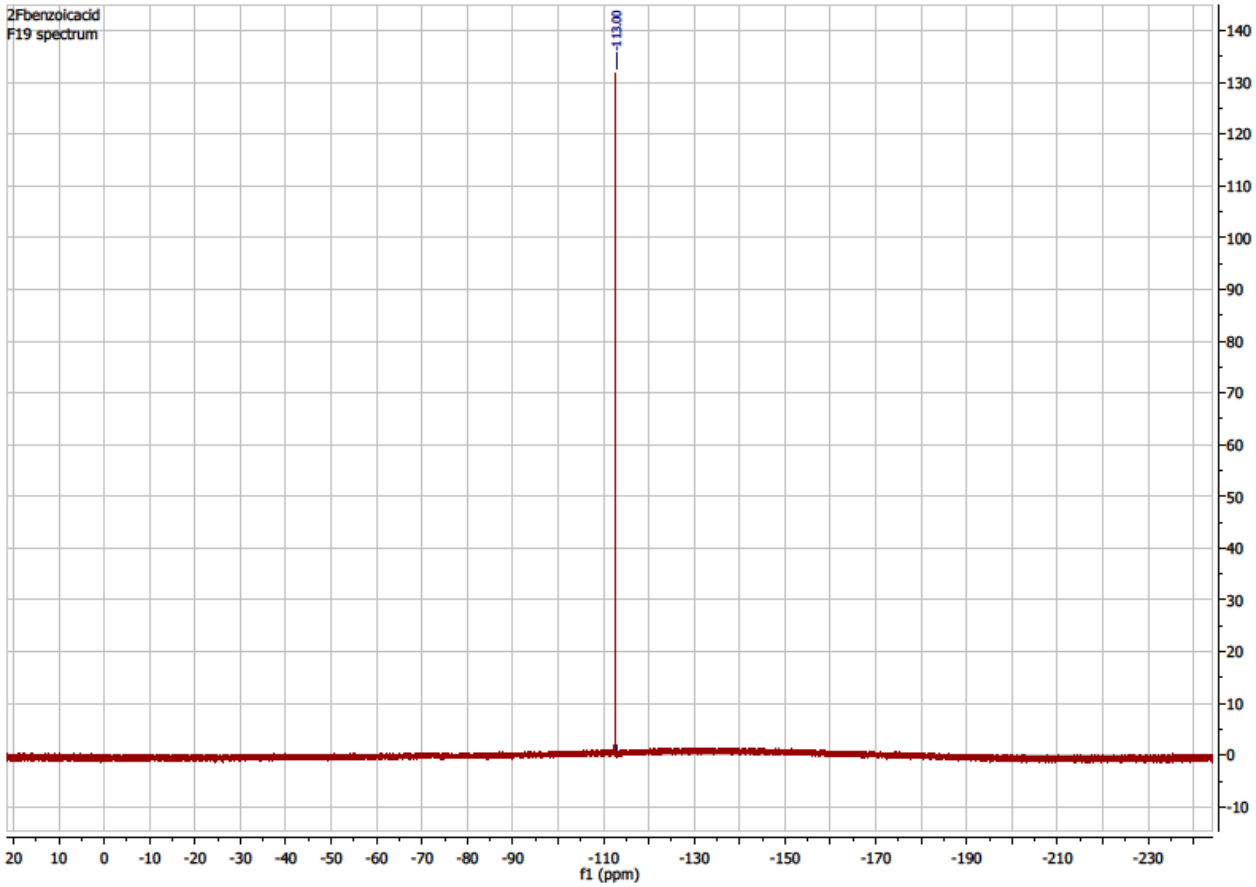

Figure S1C. ^{19}F NMR spectra for 2F-benzamide at -113.58ppm

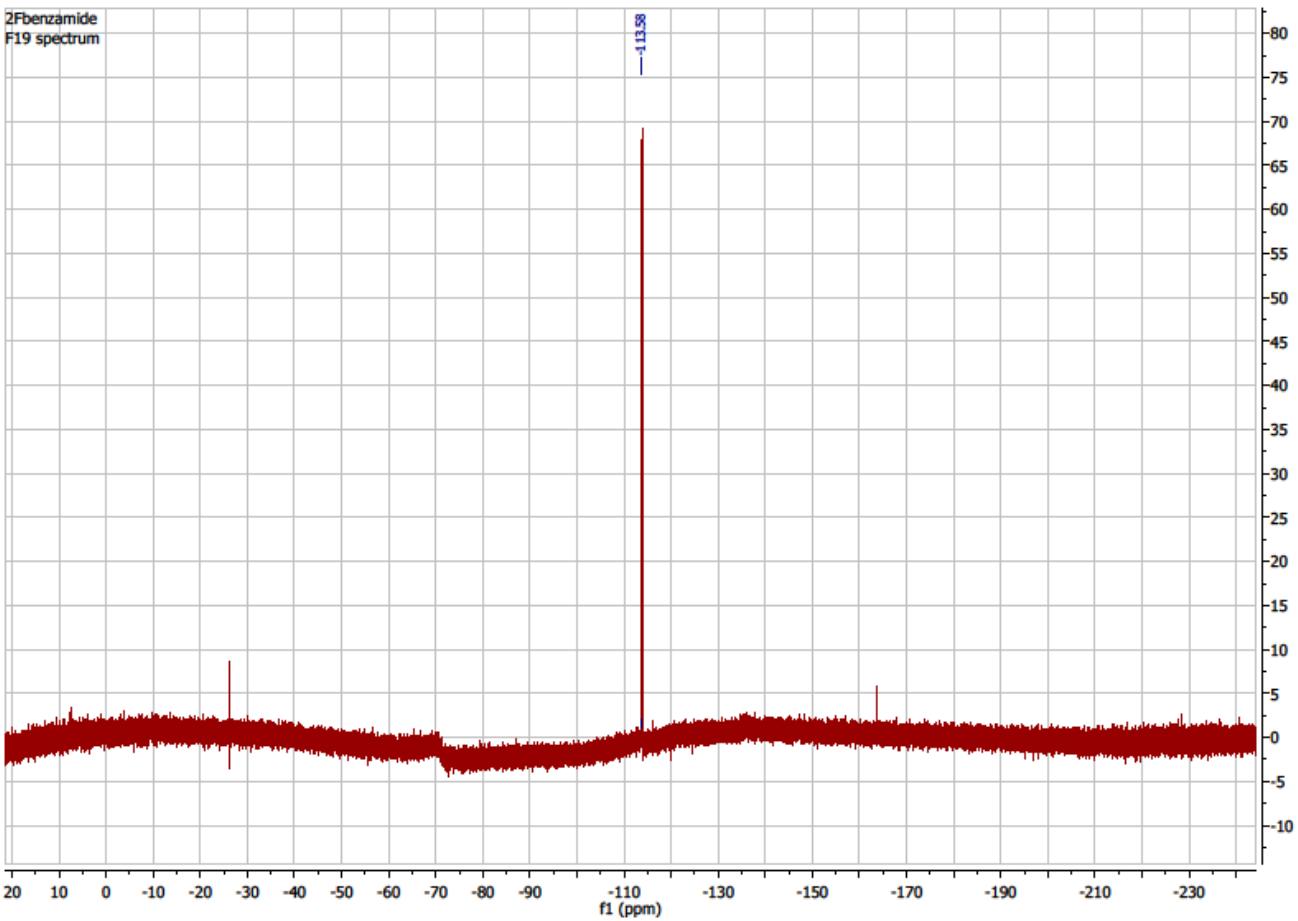

Figure S1D. ^{19}F NMR spectra for 2F-benzaldehyde at -121.32ppm

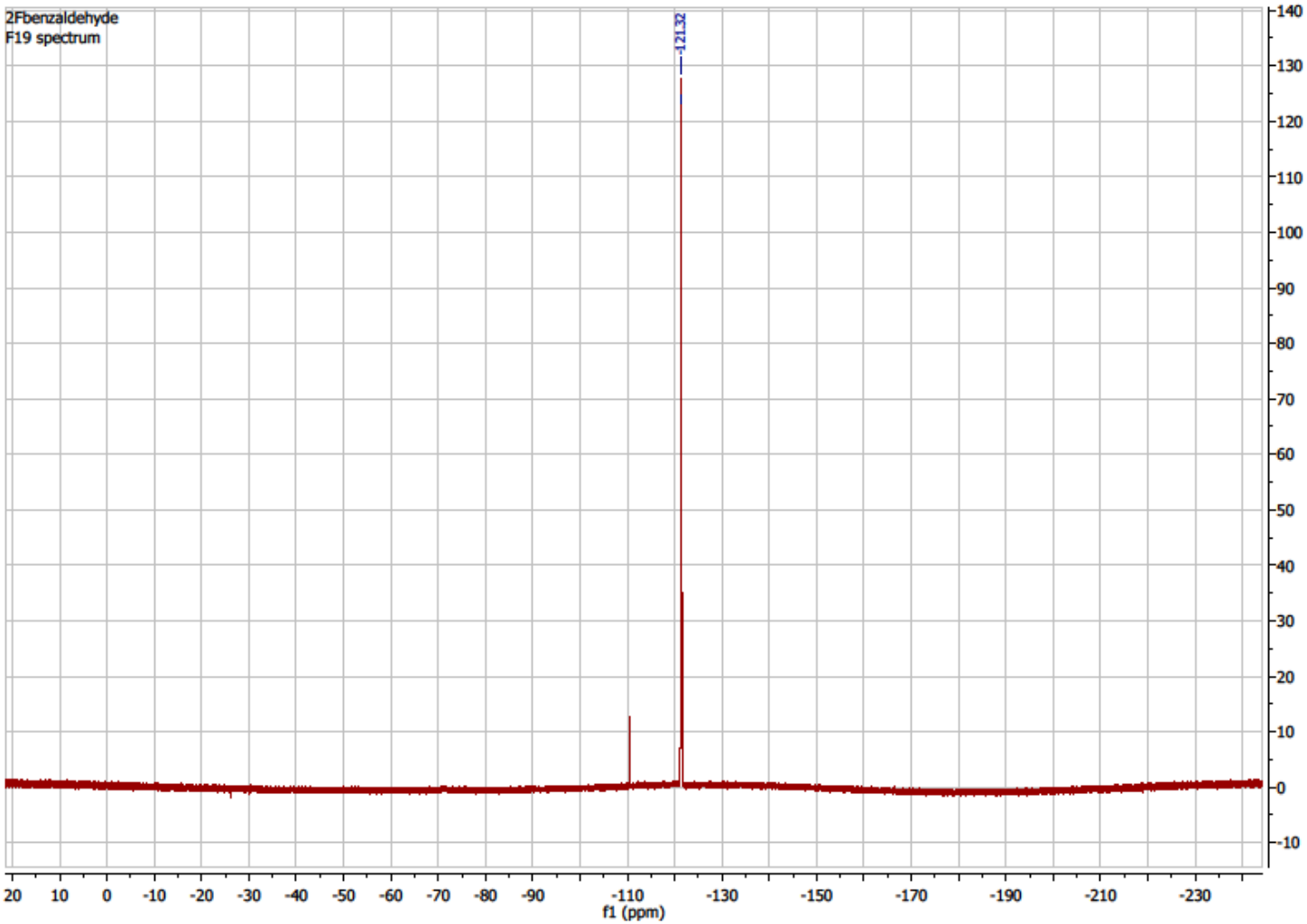

Figure S2. ^{19}F NMR spectra for 2FBzAHA incubated with NAD+ and SIRT1. Peak at -114.89 ppm is parent compound, peak at -231.88 is presumed to be intermediate. Additionally, this peak does not match any of the expected metabolites (2F-benzoic Acid, 2F-benzaldehyde, or 2F-benzamide) and represents a terminal –CH2F formation. Each peak is expanded in smaller windows.

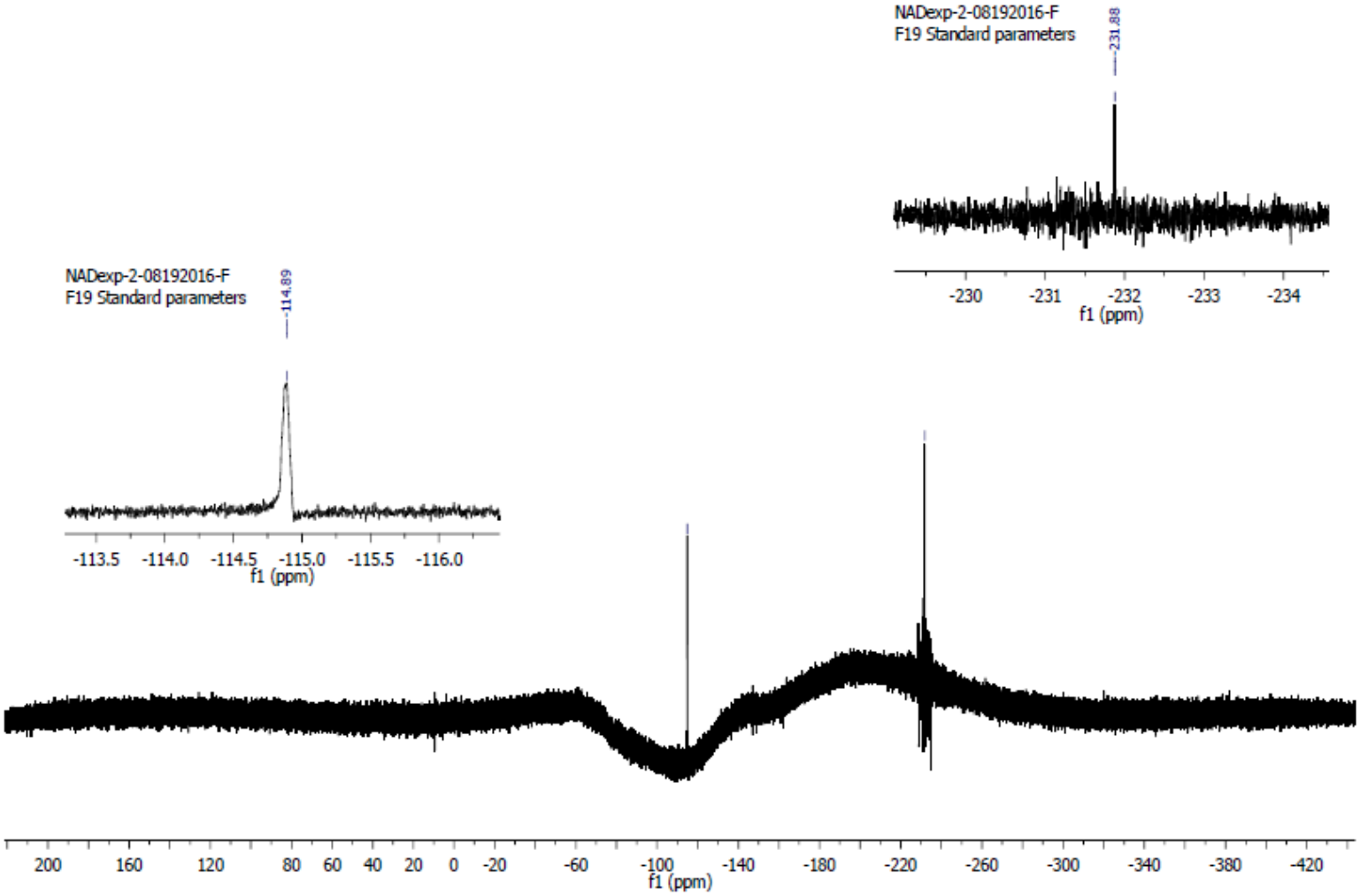

Figure S3. Dynamic PET imaging with 2-[^{18}F]BzAHA, demonstrating immediate BBB penetration of the tracer within 2 minutes post i.v. administration.

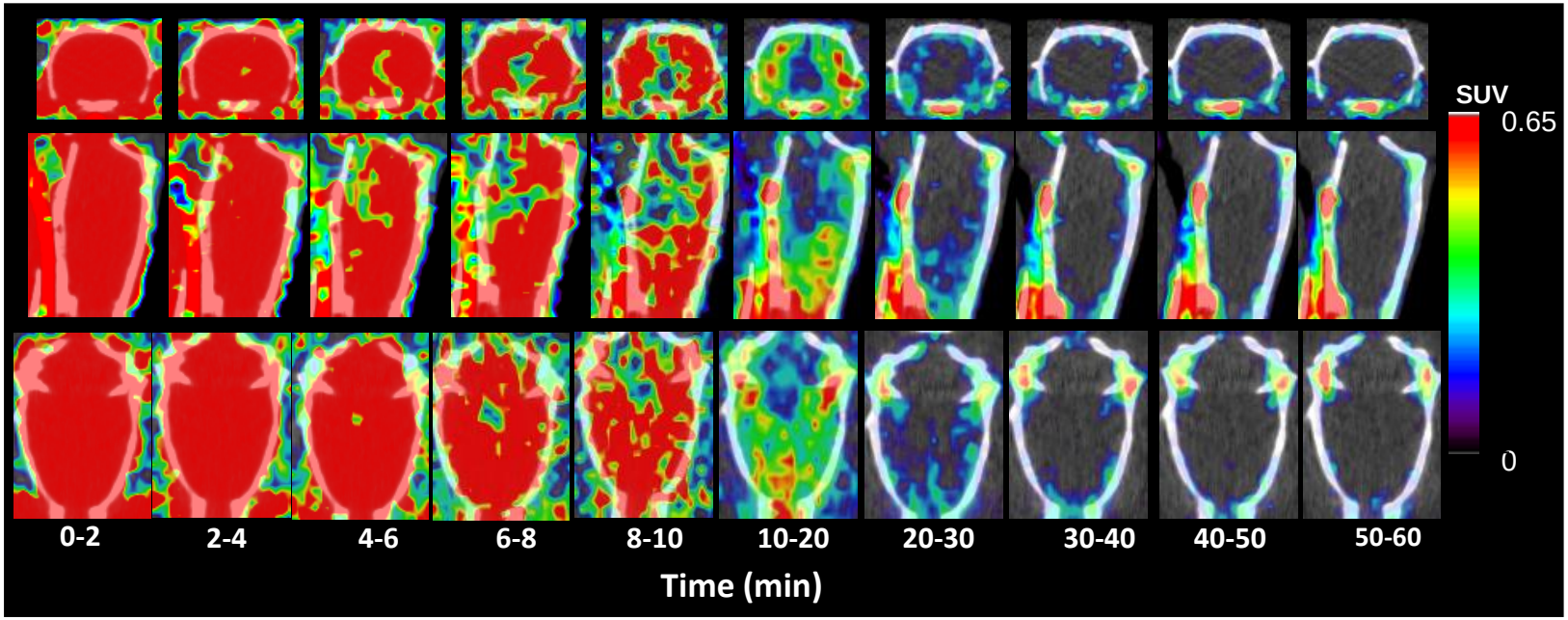

Figure S4.

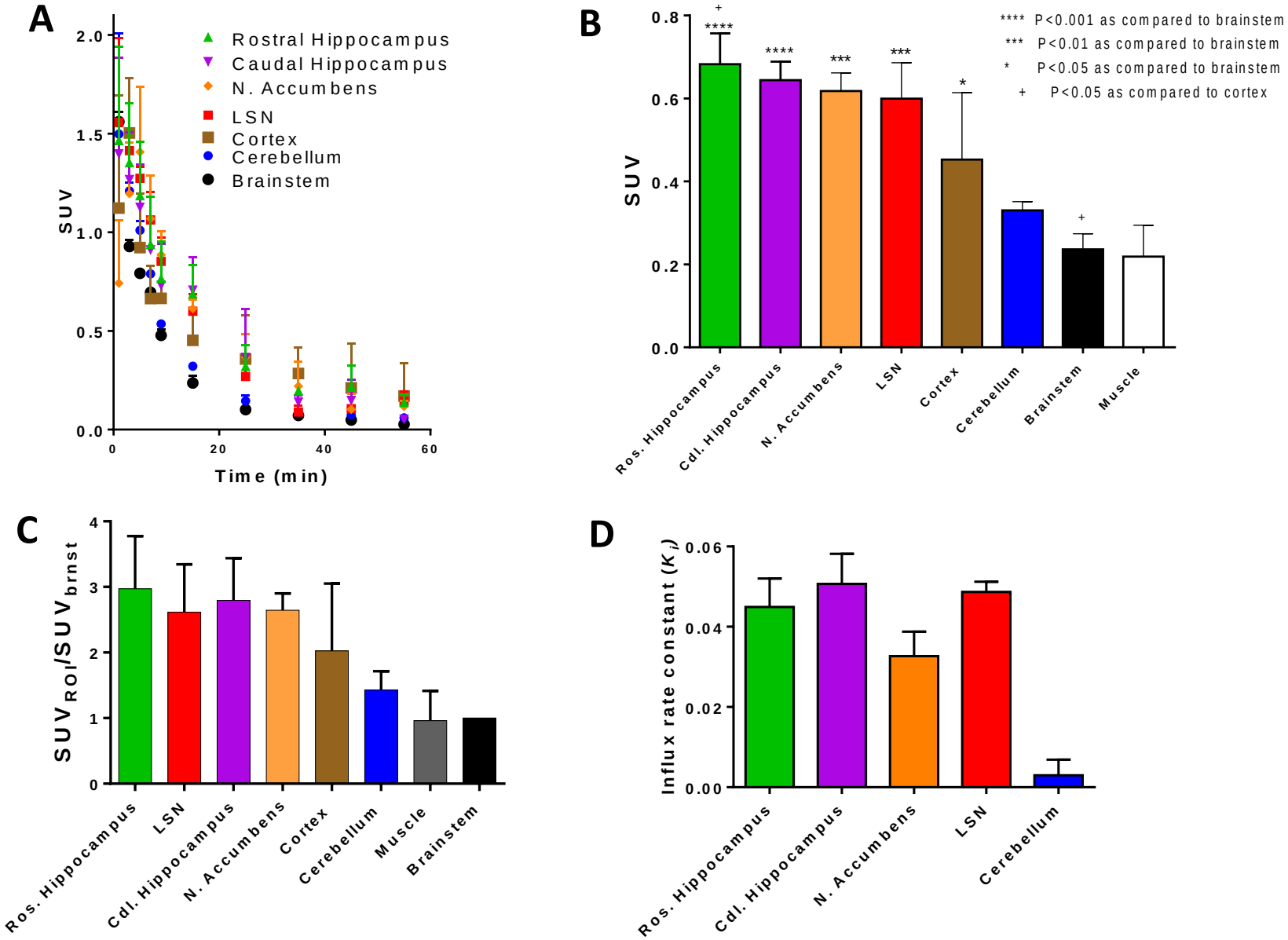

A) Time activity curves for 2-[^{18}F]BzAHA accumulation within ROIs of the brain presented as SUV vs time (60 min post i.v. administration). **B**) 2-[^{18}F]BzAHA accumulation at 20 minutes post i.v. administration with regions compared to the brainstem. **C**) Normalized SUV values for specific ROI's using brainstem as reference tissue (i.e. brainstem = 1). **D**) Ki values for specific ROI's during initial 15 minutes post tracer administration derived from Patlak graphical analysis with brainstem as reference tissue.

Figure S5. Patlak graphical analysis for 2-[^{18}F]BzAHA using brainstem as a reference tissue (N=3).

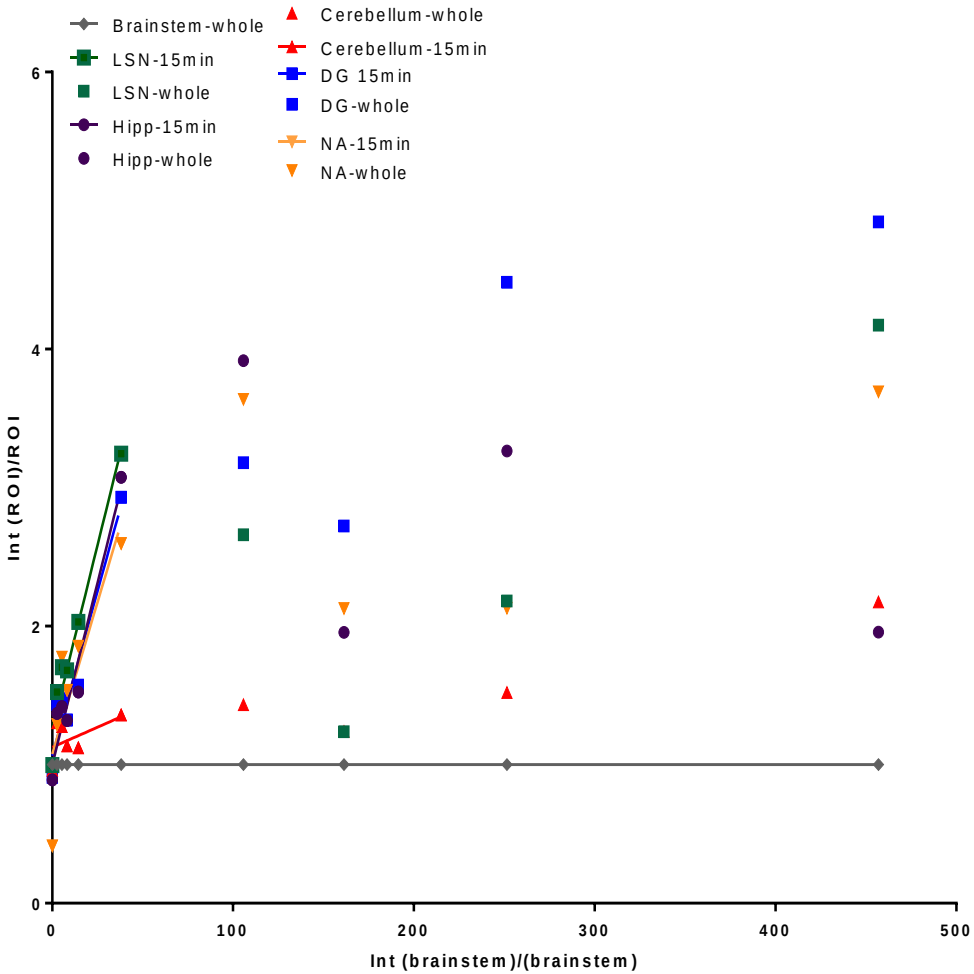

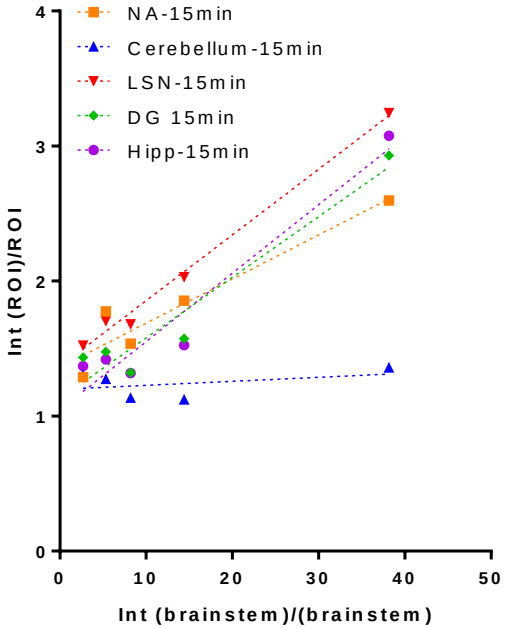

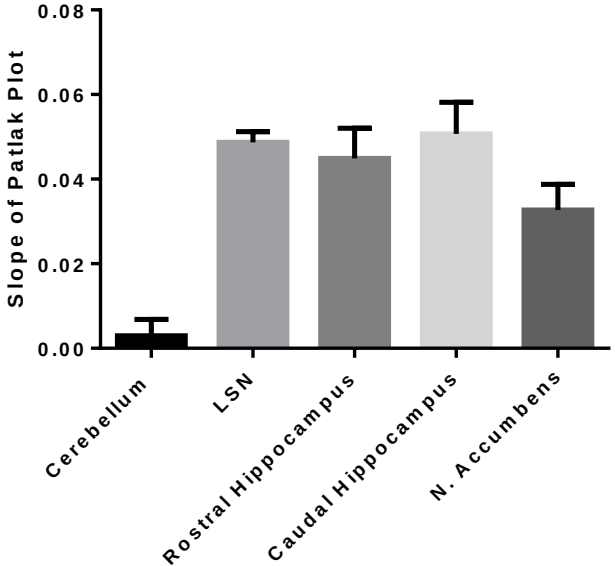

Figure S6. Time activity curves for the parent compound and radiolabeled metabolites after i.v. administration of [^{18}F]2FBzAHA in Sprague Dawley rats (N=3).

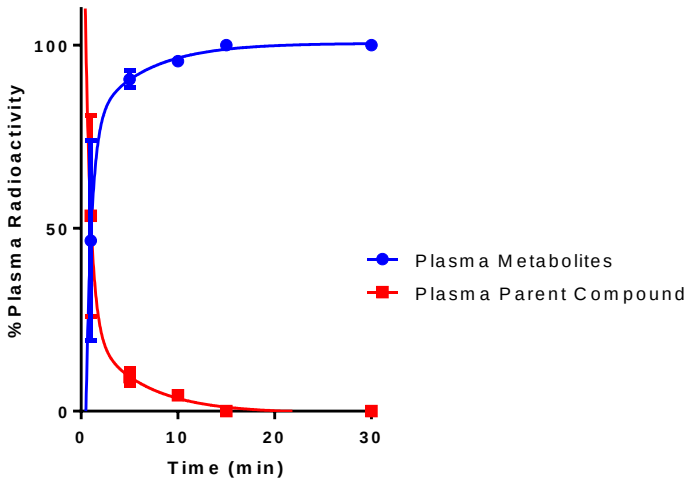

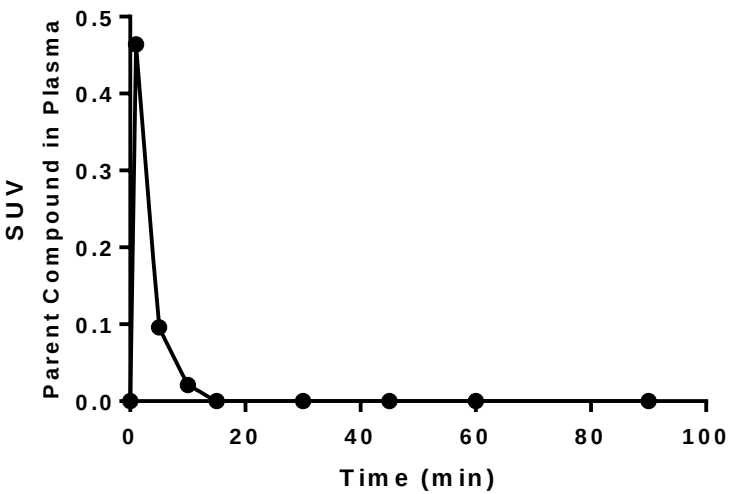

Half Life (Slow)	3.844	3.844
Goodness of Fit		
Degrees of Freedom	5	5
R square	0.8434	0.8434
Absolute Sum of Squares	763.6	763.6
Sy.x	12.36	12.36

Figure S7. Logan plot for the first 30 minutes of dynamic PET imaging, using brainstem as reference tissue for each of the brain ROI and muscle tissue (N=3)

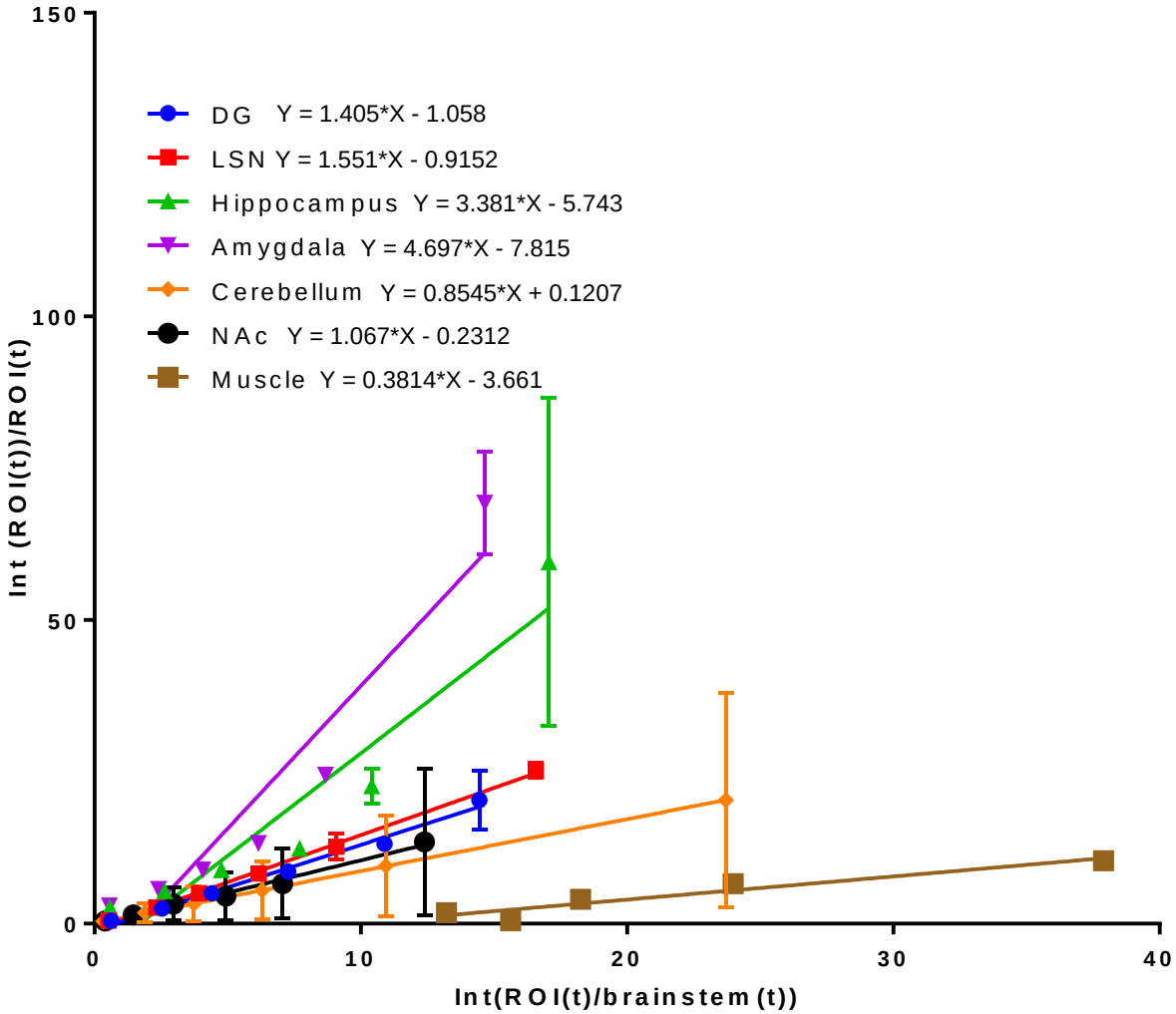

Figure S8. SIRT1 and phospho-SIRT1 expression in the CA2-CA3 region of hippocampus.

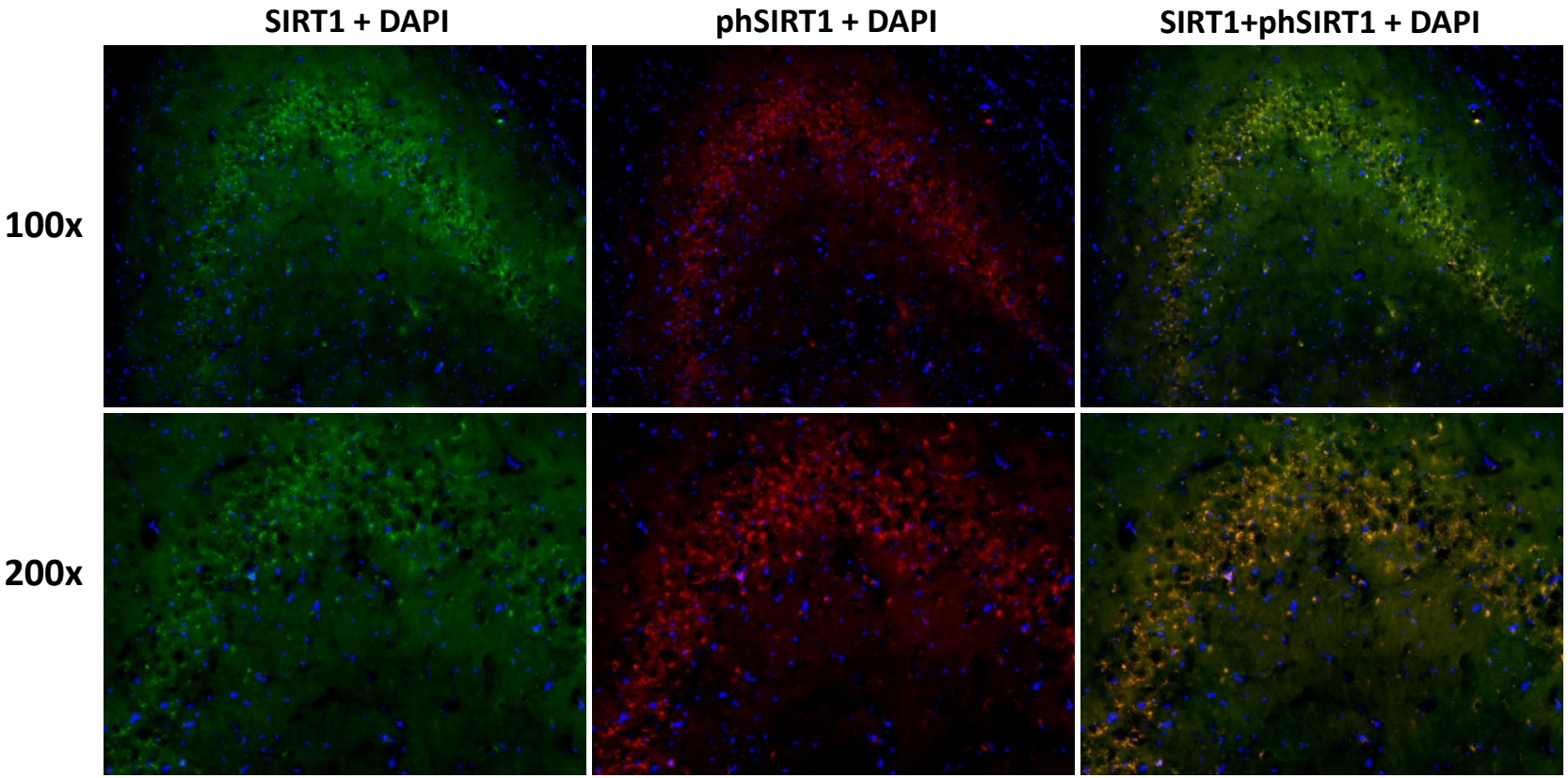

Figure S9. SIRT1 expression in axons of CA2 neurons going into the alveus and Schaffer collateral pathways.

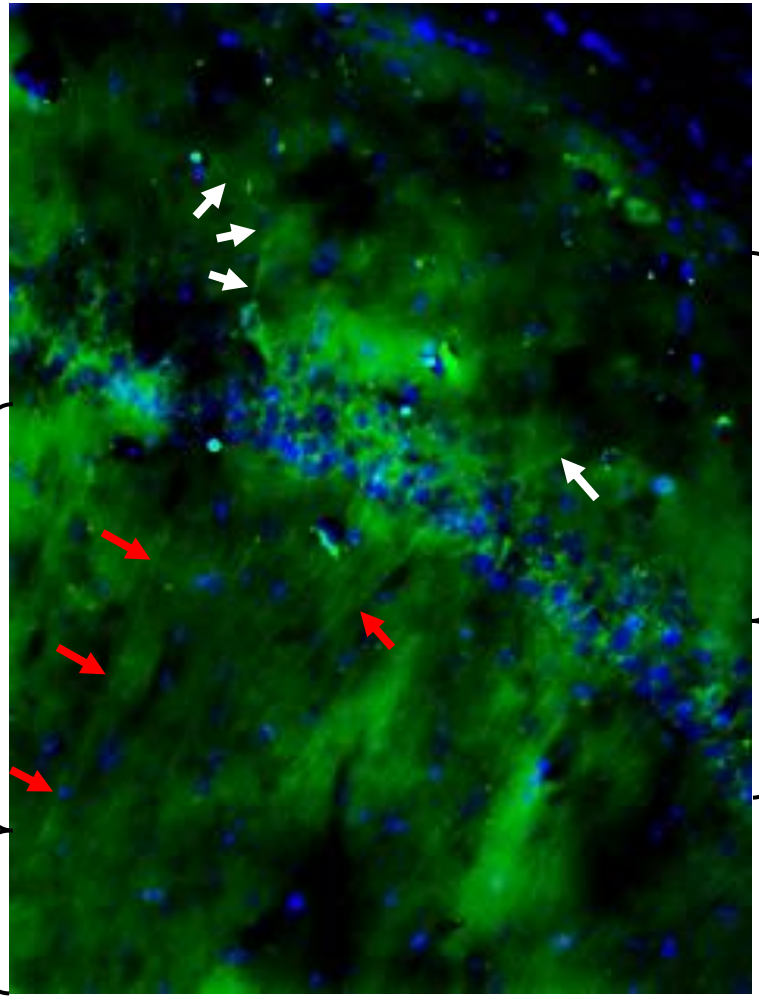

Figure S10. SIRT1 expression in dentate gyrus, in the progenitor cells of subgranular zone (SGZ)

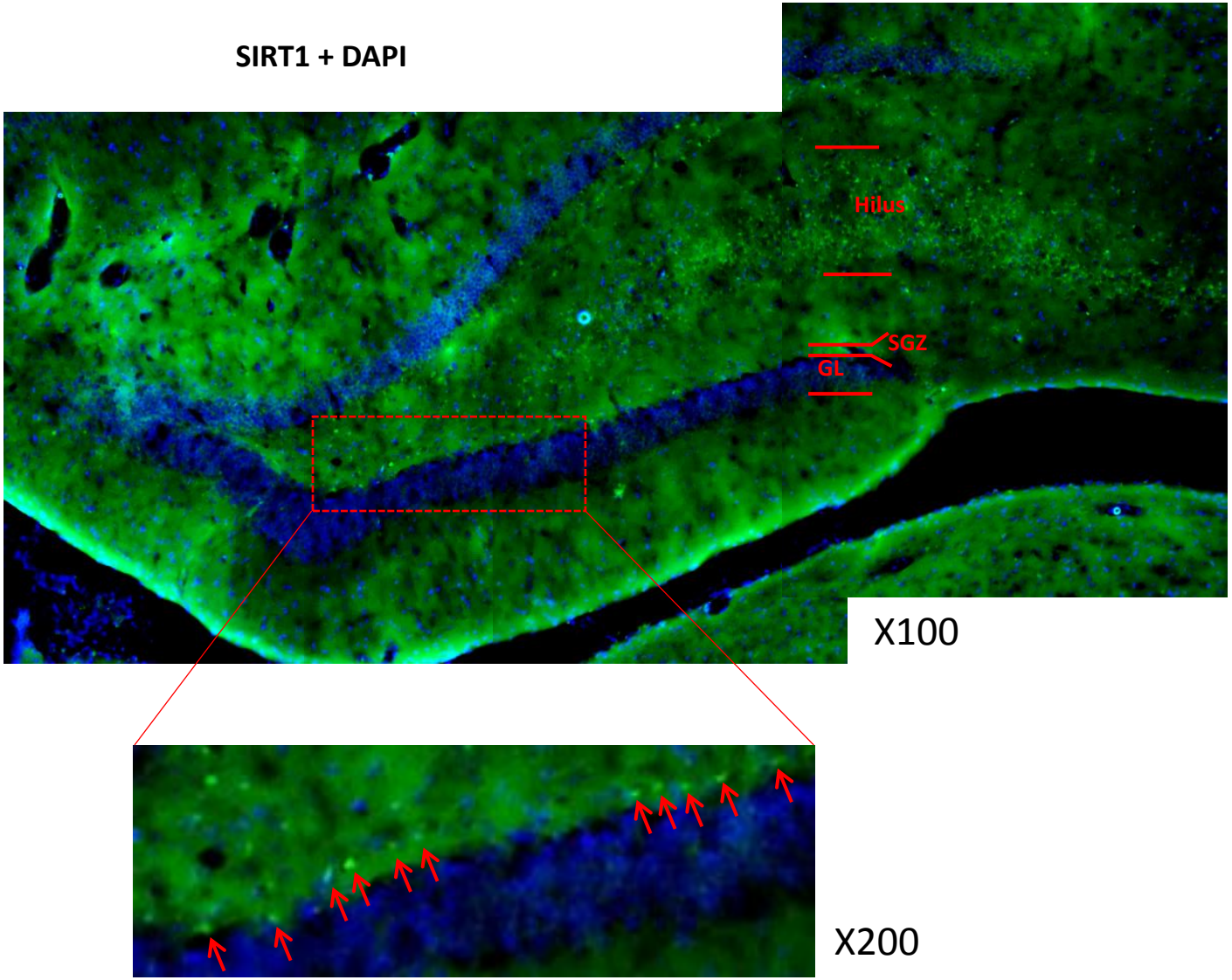

Figure S11. SIRT1 expression in the nucleus accumbens.

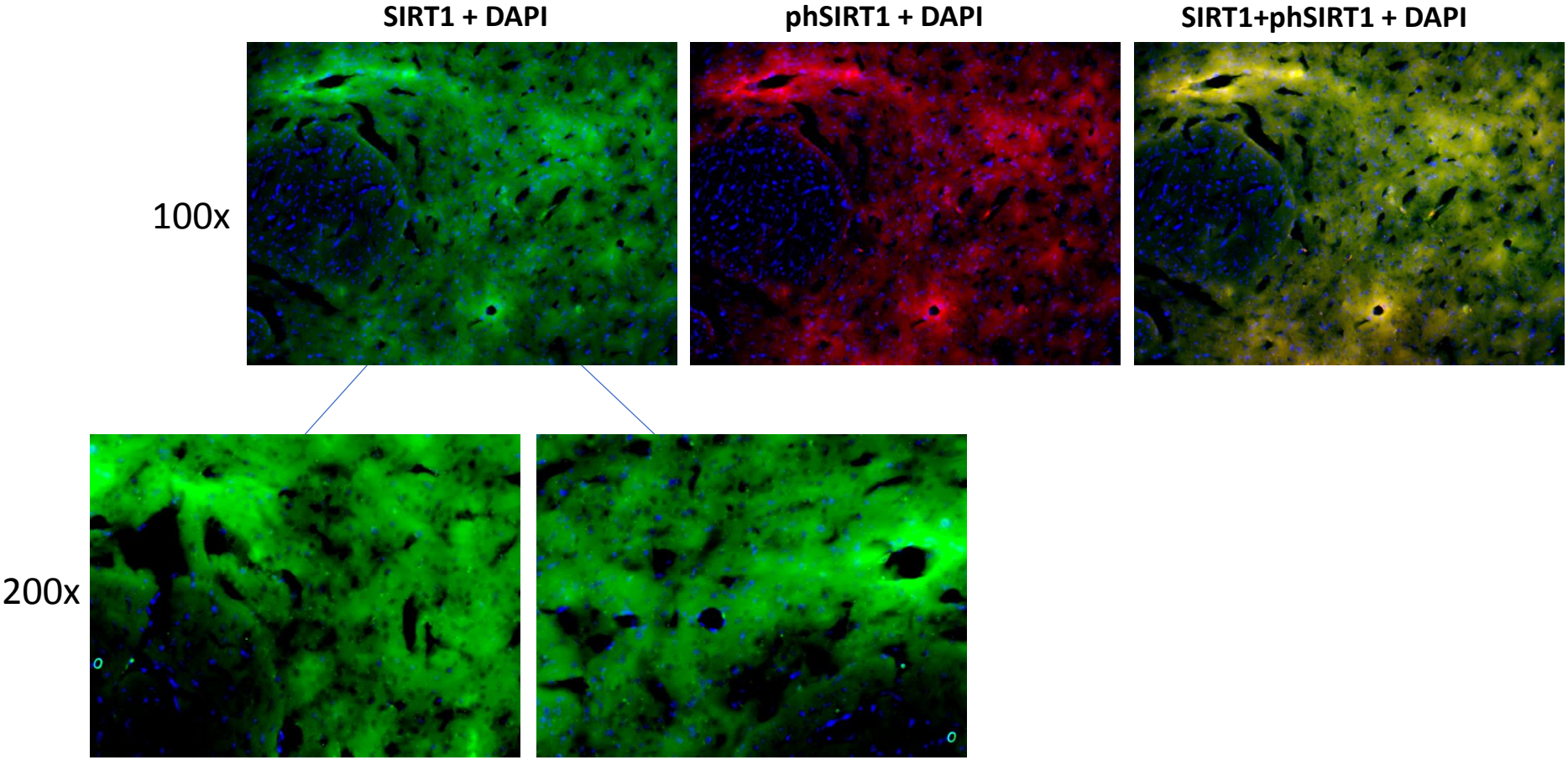

Figure S12. SIRT1 and phospho-SIRT1 expression in the cerebral cortex.

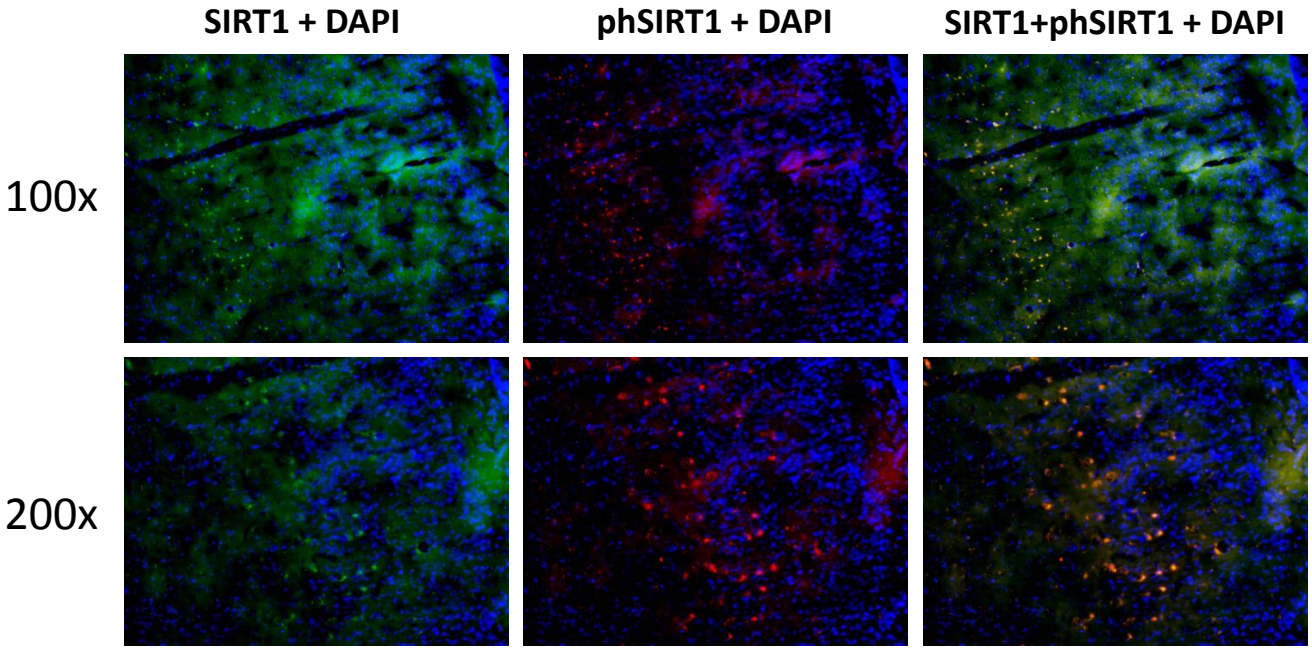

Figure S13. SIRT1 and phospho-SIRT1 expression in pericytes.

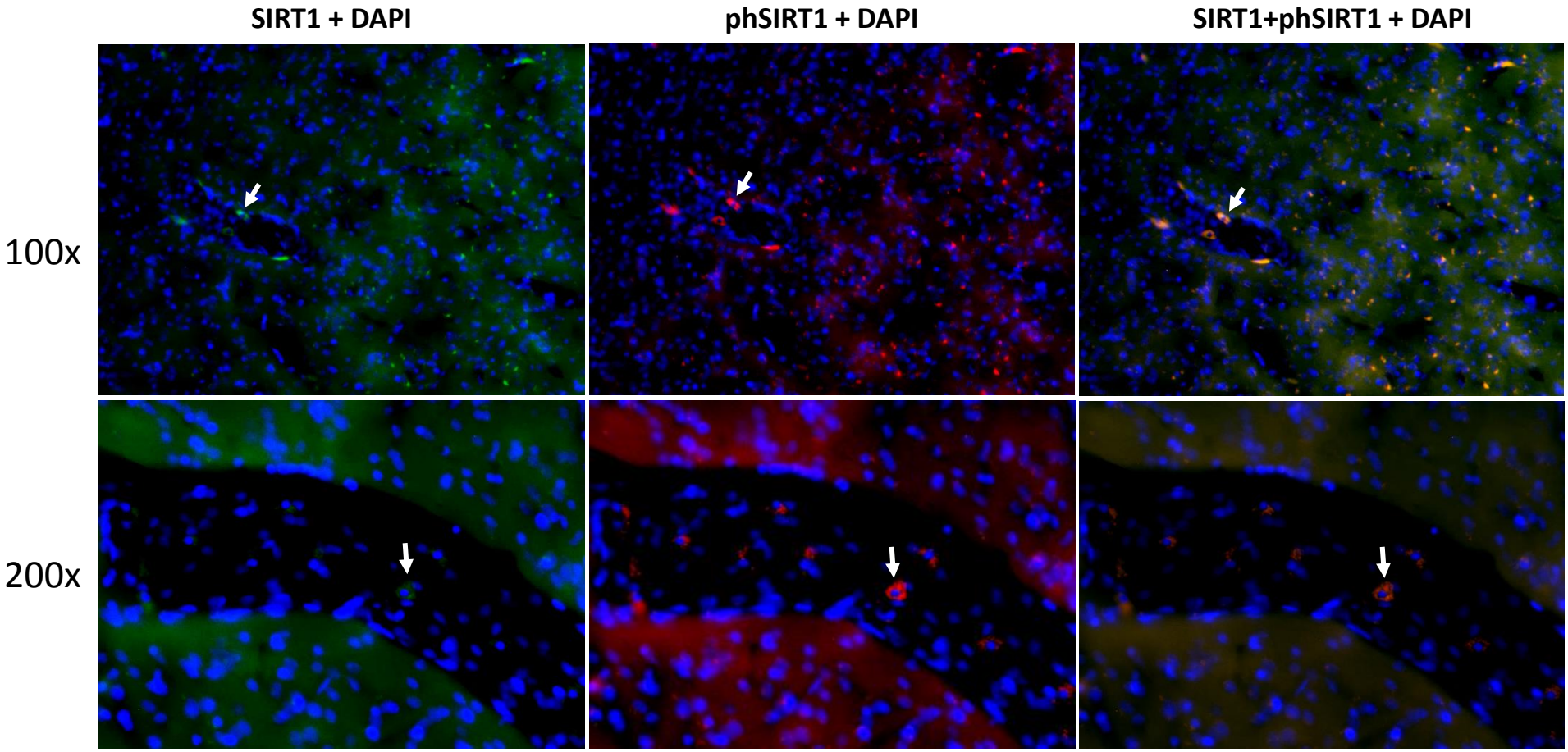

Figure S14. Autoradiographic images at 20min post i.v. administration of 2-[^{18}F]BzAHA.

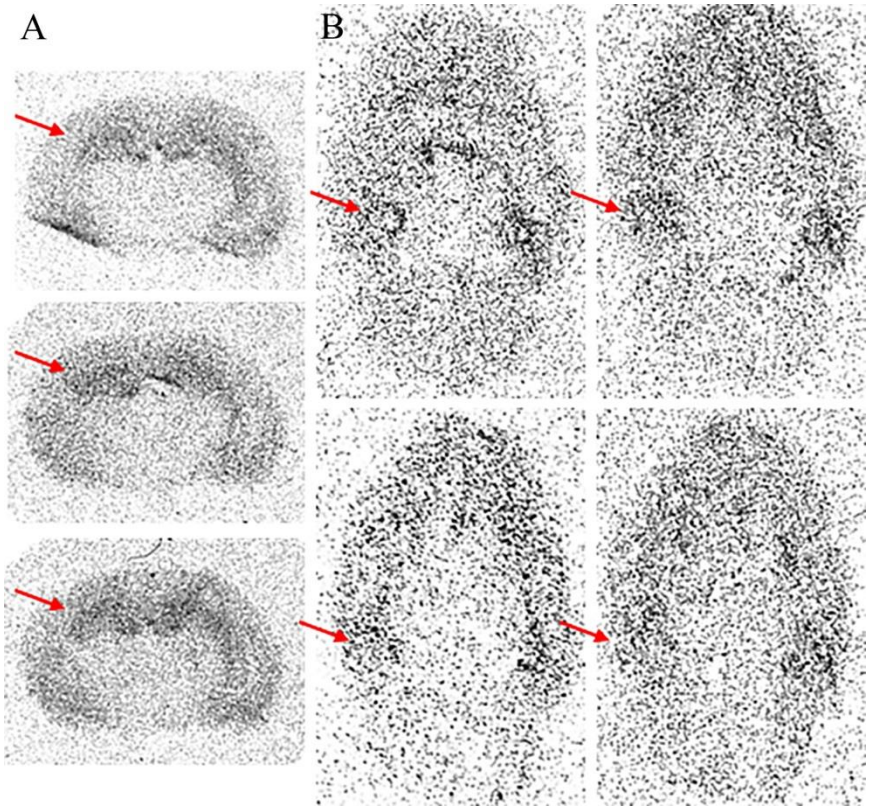

Figure S15. The mechanism of SIRT1-mediated cleavage of an acetyl group from ε-amino terminus of lysine and hypothetical/known mechanism of cleavage and transfer of phenyl/benzyl groups by SIRT1

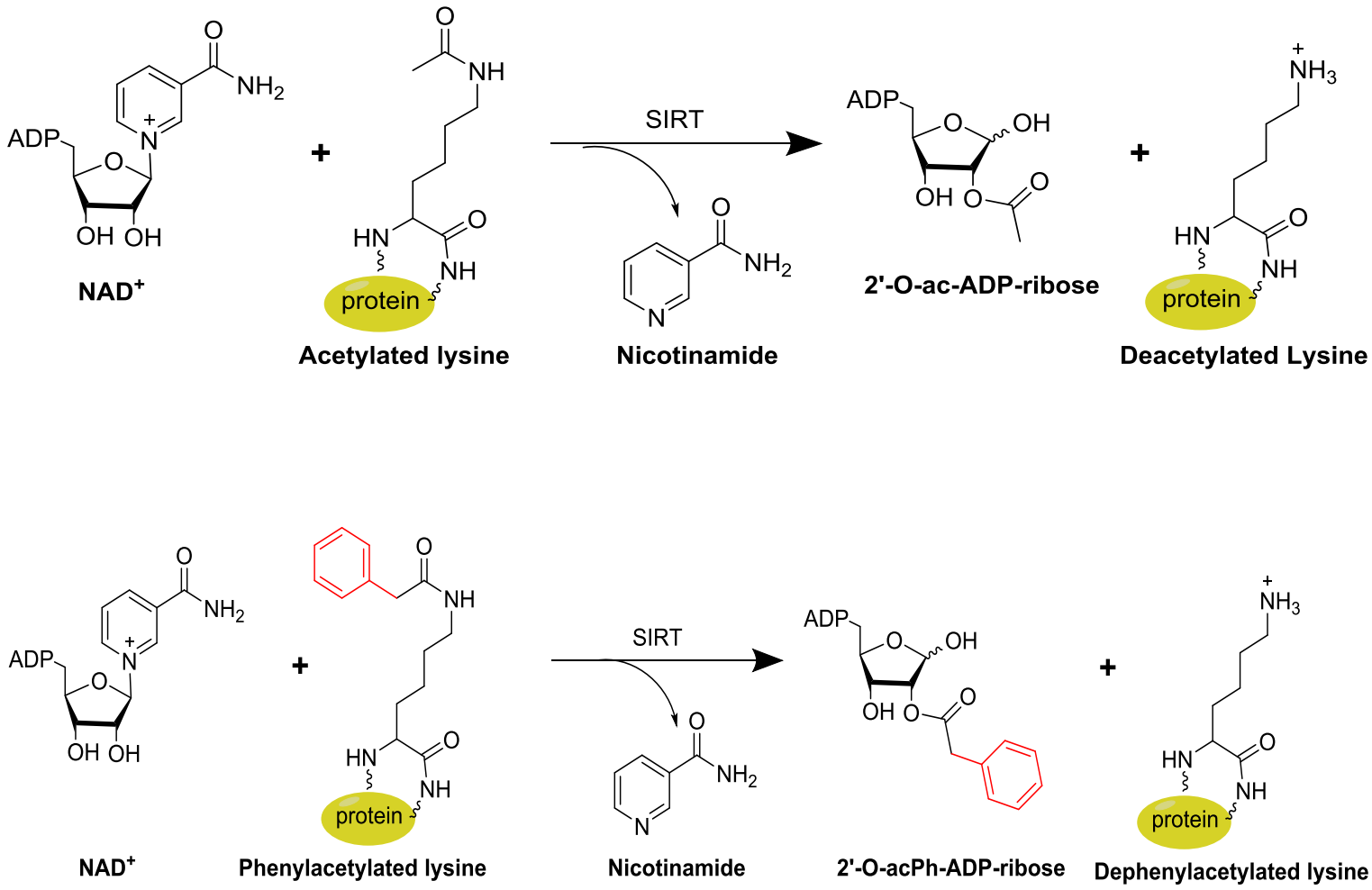

Figure S16A. Radiosynthesis of possible metabolites for *in vivo* imaging.

The starting materials were purchased and used without further purification from Sigma (Milwaukee, WI).

Synthesis of 2-[^{18}F] ethylbenzoate

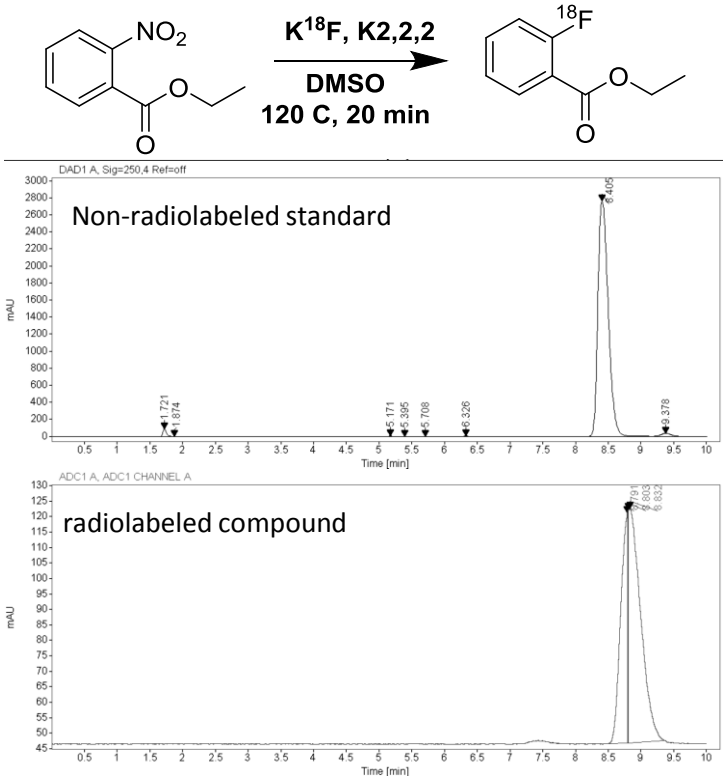

Synthesis of 2-[^{18}F] benzaldehyde

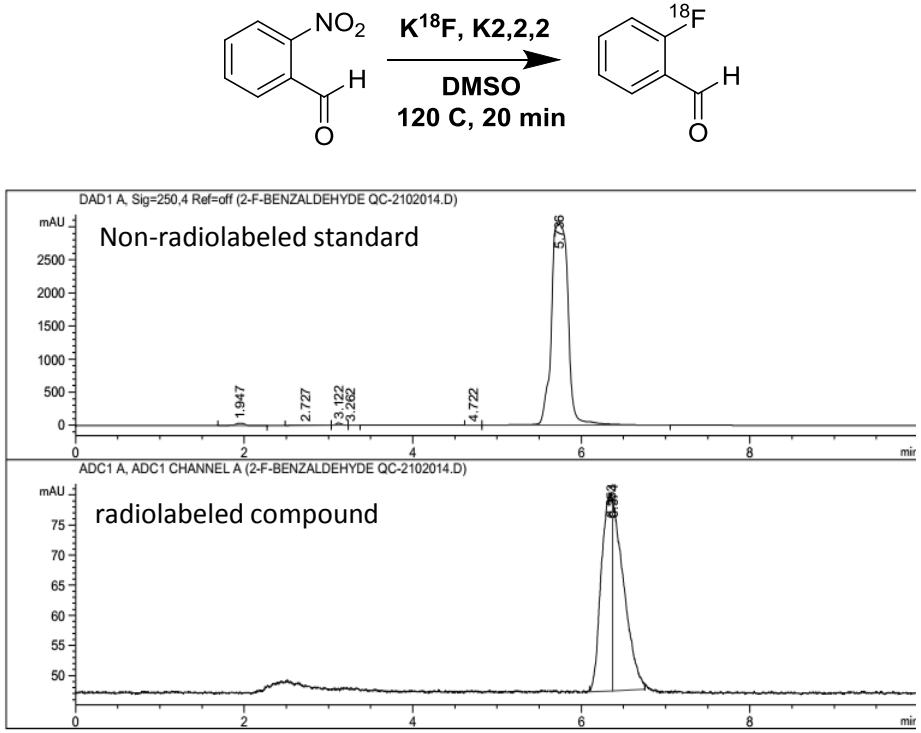

Delay in elution times between standard (top) and radiolabeled compound (bottom) is due to distance between the two detectors.

Figure S16B. Dynamic PET imaging with 2-[^{18}F]BzAHA and potential metabolites: 2-[^{18}F]Benzaldehyde and 2-[^{18}F]ethylbenzoate. The different patterns of intracerebral radioactivity accumulation demonstrated by these three tracers indicates that it is unlikely the radioactive metabolites in blood are accumulating significantly to the regional accumulation of radioactivity seen with 2-[^{18}F]BzAHA . Most notably, there is a relative absence of radioactivity in the brainstem post i.v. administration of 2-[^{18}F]BzAHA, where as there is significantly more with 2-[^{18}F]Benzaldehyde.

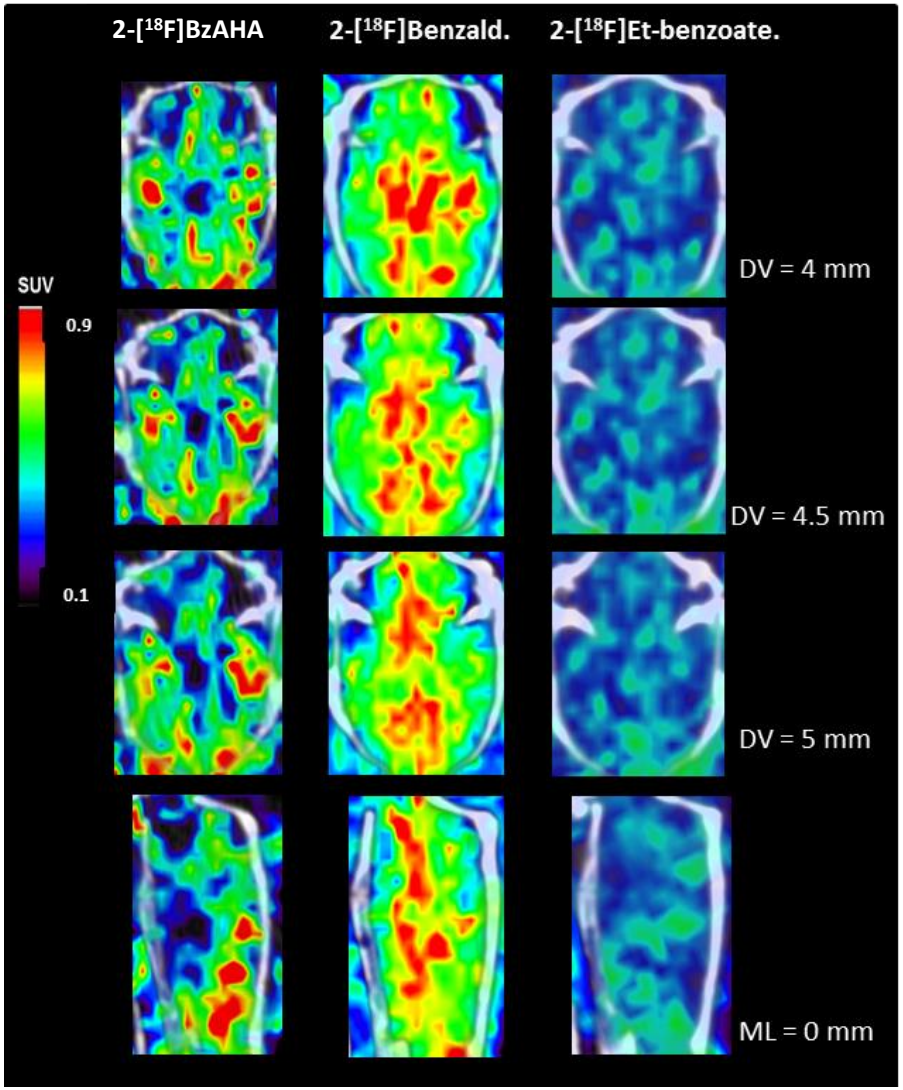

Additional Discussion of IHC Results

Observations of mixed nuclear and perinuclear localization of total SIRT1 are consistent with previous report by Ma et al., (Ma, Dong et al. 2015), but are in contrast to a report by Zakhary et al. (Zakhary, Ayubcha et al. 2010) demonstrating mostly nuclear localization of SIRT1 in the rat and human CNS. Although, SIRT1 shuttles between the nucleus and cytoplasm, playing important regulatory roles in both cellular compartments (Michan and Sinclair 2007), phosphorylation on the N-terminal S27 and S47 of SIRT1 has been associated with its nuclear localization (Nasrin, Kaushik et al. 2009). Furthermore, phosphorylation of SIRT1 at S47 as indicated an increase in SIRT1 activity, particularly within the JNK pathway (Lau, Liu et al. 2014). Also, it has been established that NAD+-dependent deacetylase activity of SIRT1 is modulated by phosphorylation (Sasaki, Maier et al. 2008). Therefore, the observed perinuclear localization of phospho-SIRT1 in the current study needs further investigation.

Literature Cited:

Lau, A. W., P. Liu, H. Inuzuka and D. Gao (2014). "SIRT1 phosphorylation by AMP-activated protein kinase regulates p53 acetylation." American Journal of Cancer Research **4**(3): 245-255.

Ma, L., W. Dong, R. Wang, Y. Li, B. Xu, J. Zhang, Z. Zhao and Y. Wang (2015). "Effect of caloric restriction on the SIRT1/mTOR signaling pathways in senile mice." Brain Res Bull **116**: 67-72.

Michan, S. and D. Sinclair (2007). "Sirtuins in mammals: insights into their biological function." Biochem J **404**(1): 1-13.

Nasrin, N., V. K. Kaushik, E. Fortier, D. Wall, K. J. Pearson, R. de Cabo and L. Bordone (2009). "JNK1 phosphorylates SIRT1 and promotes its enzymatic activity." PLoS One **4**(12): e8414.

Sasaki, T., B. Maier, K. D. Koclega, M. Chruszcz, W. Gluba, P. T. Stukenberg, W. Minor and H. Scrable (2008). "Phosphorylation regulates SIRT1 function." PloS one **3**(12).

Zakhary, S. M., D. Ayubcha, J. N. Dileo, R. Jose, J. R. Leheste, J. M. Horowitz and G. Torres (2010). "Distribution analysis of deacetylase SIRT1 in rodent and human nervous systems." The Anatomical Record **293**(6): 1024-1032.